Manipulating the ABCs of self-assembly via low-χ block polymer design

Alice B. Chang[a], Christopher M. Bates[b,c,1], Byeongdu Lee[d], Carol M. Garland[e], Simon C. Jones[f], Russell K. W. Spencer[g,h,i], Mark W. Matsen[g,h,i,1], and Robert H. Grubbs[a,1]

[a]Arnold and Mabel Beckman Laboratories for Chemical Synthesis, California Institute of Technology, Pasadena, CA 91125; [b]Materials Department, University of California, Santa Barbara, CA 93106; [c]Department of Chemical Engineering, University of California, Santa Barbara, CA 93106; [d]X-Ray Science Division, Advanced Photon Source, Argonne National Laboratory, Argonne, IL 60439; [e]Department of Materials Science, California Institute of Technology, Pasadena, CA 91125; [f]Electrochemical Technologies Group, Jet Propulsion Laboratory, California Institute of Technology, Pasadena, CA 91109; [g]Department of Chemical Engineering, University of Waterloo, Waterloo, ON N2L 3G1, Canada; [h]Department of Physics & Astronomy, University of Waterloo, Waterloo, ON N2L 3G1, Canada; and [i]Waterloo Institute for Nanotechnology, University of Waterloo, Waterloo, ON N2L 3G1, Canada

Contributed by Robert H. Grubbs, May 7, 2017 (sent for review January 25, 2017; reviewed by Thomas Epps and Edwin L. Thomas)

Block polymer self-assembly typically translates molecular chain connectivity into mesoscale structure by exploiting incompatible blocks with large interaction parameters (χ_{ij}). In this article, we demonstrate that the converse approach, encoding low-χ interactions in ABC bottlebrush triblock terpolymers ($\chi_{AC} \lesssim 0$), promotes organization into a unique mixed-domain lamellar morphology, which we designate LAM$_P$. Transmission electron microscopy indicates that LAM$_P$ exhibits ACBC domain connectivity, in contrast to conventional three-domain lamellae (LAM$_3$) with ABCB periods. Complementary small-angle X-ray scattering experiments reveal a strongly decreasing domain spacing with increasing total molar mass. Self-consistent field theory reinforces these observations and predicts that LAM$_P$ is thermodynamically stable below a critical χ_{AC}, above which LAM$_3$ emerges. Both experiments and theory expose close analogies to ABA′ triblock copolymer phase behavior, collectively suggesting that low-χ interactions between chemically similar or distinct blocks intimately influence self-assembly. These conclusions provide fresh opportunities for block polymer design with potential consequences spanning all self-assembling soft materials.

block polymer | self-assembly | polymer nanostructure | domain spacing | LAM$_P$

Block polymers are a diverse class of soft materials capable of self-assembling into complex periodic nanostructures. Synthetic command over composition, dispersity, sequence, and molecular architecture enables control over the mesoscopic order and macroscopic thermal, mechanical, rheological, and transport properties (1–4). The phase behavior of "simple" linear AB diblock copolymers is universally parameterized by the segregation strength $\chi_{AB}N$ and relative volume fraction f, where χ_{AB} represents the effective Flory–Huggins binary interaction parameter and N is the total volume-averaged degree of polymerization. Mixing behavior, captured through the mean-field concept of χ_{AB}, is central to block polymer self-assembly: the competing demands of minimizing interfacial energy and maximizing configurational entropy only favor microphase separation when A–B interactions are repulsive ($\chi_{AB} > 0$) (5, 6). Extension to higher-order multiblock polymers introduces additional interaction parameters (χ_{ij}) that impact self-assembly and properties (7). For example, introducing a mutually incompatible C block ($\chi_{AC} > 0$, $\chi_{BC} > 0$) generates a host of new morphologies dictated by the chain connectivity (ABC, ACB, or BAC) and intrinsic χ_{ij}-values (8, 9). In this rich phase space, designing multiblock polymers with a combination of miscible and immiscible blocks can also access new structures and impart useful functions (10, 11). Perhaps the best-known examples of such systems are linear ABA′ triblock copolymers ($\chi_{AB} > 0$, $\chi_{AA'} \approx 0$): their high-value industrial applications as thermoplastic elastomers are entirely enabled by A/A′ mixing and chain connectivity, which together create physically cross-linked materials with excellent processability and mechanical properties (12). The self-assembly of yet more complex systems, including ABA′C tetrablock polymers (13, 14) and $A_n(BA')_m$ heteroarm star polymers (15), is also crucially determined by A/A′ miscibility. These examples illuminate interesting parallels and contrasts between block polymer phase behavior and protein self-assembly. Nature delivers exquisite control over protein folding by precisely tailoring amino acid sequences and intramolecular interactions that are often attractive (e.g., hydrogen bonding), whereas block polymer design to date exploits simple molecular connectivity and primarily repulsive interactions ($\chi > 0$) to induce microphase separation.

Previous reports have investigated the role of negligible ($\chi \sim 0$) or attractive ($\chi < 0$) intermolecular interactions on the phase behavior of various homopolymer (AB/A′) (16, 17) and block polymer (AB/A′C) (18, 19) blends. In contrast, studies in which the macromolecules themselves are intramolecularly encoded with miscible blocks are to the best of our knowledge limited to the aforementioned A/A′ self-similar interactions. In this report, we study ABC bottlebrush triblock terpolymers with grafted poly(D,L-lactide), poly(styrene), and poly(ethylene oxide) side chains (LSO), featuring low-χ interactions ($\chi_{AC} \lesssim 0$) between distinct A and C end blocks. These materials generate a unique mixed morphology with atypical mesoscopic domain connectivity, which we denote LAM$_P$. Additionally, under certain conditions of molecular asymmetry, another consequence of low-χ design manifests in decreasing domain spacing with increasing total molar mass.

Significance

Molecular sequence and interactions dictate the mesoscale structure of all self-assembling soft materials. Block polymers harness this relationship to access a rich variety of nanostructured materials but typically require energetically unfavorable (high-χ) interactions between blocks. Contrary to this convention, we demonstrate that ABC triblock terpolymers featuring low-χ interactions between end blocks can self-assemble into a unique mixed morphology that subverts the demands of chain connectivity. As a consequence of block–block mixing, the characteristic length scales of these self-assembled structures exhibit an unusual trend: As the total polymer size increases, the domain spacing decreases. These developments expand the vocabulary of block polymer design and open additional avenues for manipulating the self-assembly of synthetic macromolecules.

Author contributions: A.B.C., C.M.B., and R.H.G. designed research; A.B.C., S.C.J., R.K.W.S., and M.W.M. performed research; A.B.C., B.L., C.M.G., S.C.J., R.K.W.S., and M.W.M. contributed new reagents/analytic tools; A.B.C., C.M.B., B.L., and M.W.M. analyzed data; R.H.G. directed and served as principal investigator and discussed interpretation of the results; and A.B.C. and C.M.B. wrote the paper.

Reviewers: T.E., University of Delaware; and E.L.T., Rice University.

The authors declare no conflict of interest.

[1]To whom correspondence may be addressed. Email: bates@engr.ucsb.edu, mwmatsen@uwaterloo.ca, or rhg@caltech.edu.

This article contains supporting information online at www.pnas.org/lookup/suppl/doi:10.1073/pnas.1701386114/-/DCSupplemental.

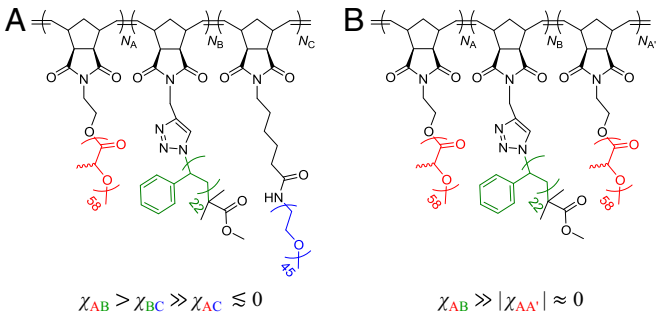

Fig. 1. Molecular structures and relative interaction parameters for (*A*) LSO and (*B*) LSL′ brush triblock polymers.

Valuable insight into the molecular origins of this unusual behavior is achieved by comparison with analogous ABA′ brush triblock copolymers—grafted poly(D,L-lactide)-*block*-poly(styrene)-*block*-poly(D,L-lactide) (LSL′)—and self-consistent field theory (SCFT). The experimental and theoretical conclusions described herein regarding low-χ block polymers reveal unexpected breadth in self-assembly and should create new opportunities for molecular and materials design.

Results and Discussion

Synthesis and Structure of Low-χ Block Polymers. ABC and ABA′ brush triblock polymers containing grafted poly(D,L-lactide) (PLA, A block), polystyrene (PS, B block), and poly(ethylene oxide) (PEO, C block) side chains were synthesized by ring-opening metathesis polymerization (ROMP) (20–22). The living nature and synthetic utility of ROMP enable the formation of well-defined block polymers with precisely controlled molar mass, narrow molar mass dispersity, and diverse pendant functionalities. Synthetic details (*SI Appendix*, Scheme S1), characterization data (*SI Appendix*, Tables S1 and S2), and size-exclusion chromatograms (*SI Appendix*, Figs. S1–S3) for all samples are provided. Fig. 1 illustrates the molecular structure of the LSO and LSL′ brush triblock polymers studied herein and highlights the relative interaction parameters dictated by block chemistry and sequence. Both LSO and LSL′ feature low-χ interactions between the end blocks (χ_{AC}, $\chi_{AA'} \lesssim 0$), which in particular distinguish LSO from typical frustrated ABC triblock polymers that include similar relative χ-values but highly unfavorable A/C interactions ($\chi_{AC} >> 0$) (9, 23). N_A, N_B, and (N_C or $N_{A'}$) indicate the number-average degrees of polymerization through the polynorbornene backbone for blocks containing PLA, PS, and (PEO or PLA) grafts, respectively. All LSO and LSL′ triblock polymers were annealed at 140 °C under modest applied pressure, and the ordered structures that developed were identified by synchrotron small-angle X-ray scattering (SAXS) (e.g., see *SI Appendix*, Fig. S4).

SCFT. SCFT, generally regarded as the state of the art for block polymer melts (24), was used to model our polymers and provide insight into their self-assembly. The standard model for branched polymers was modified to account for the strong steric interactions that occur in bottlebrushes due to the high grafting density of the side chains, as was done previously for similar bottlebrush block polymers (25). Gaussian chains were used to represent the $N = N_A + N_B + N_C$ (LSO) or $N = N_A + N_B + N_{A'}$ (LSL′) side chains, and the volumes and unperturbed end-to-end lengths of the side chains were set to known literature values (26, 27). For the backbone, a worm-like chain of fixed persistence length was used to handle the strong lateral tension that occurs due to side-chain crowding. The interactions between the three side-chain species (PLA, PS, and PEO) were represented in the Hamiltonian by standard Flory–Huggins terms controlled by χ_{LS}, χ_{SO}, and χ_{LO}. The equilibrium lamellar period (d^*) was obtained by minimizing the free energy (F). Additional SCFT details, including values for all parameters (*SI Appendix*, Table S3) and a schematic of chain dimensions (*SI Appendix*, Scheme S2), are provided.

Unique Domain Connectivity. We begin by presenting data and calculations corresponding to LSO brush triblock terpolymers (Fig. 1*A*), then draw close analogies to LSL′ (Fig. 1*B*) phase behavior. All LSO materials self-assemble into well-ordered lamellar morphologies. Transmission electron micrographs of thin sections of LSO* ($N_A = 28$, $N_B = 27$, $N_C = 5$) stained over ruthenium tetroxide (RuO_4) vapor reveal a three-color, four-layer lamellar morphology (Fig. 2*A*). (Additional images are provided in the *SI Appendix*, Fig. S5.) Exposing L, S, and O to RuO_4 vapor results in unstained, slightly stained, and strongly stained domains, respectively, as deduced from literature results: PS is selectively stained in PLA/PS mixtures (28, 29), and PEO is stained to a greater extent than PS (30, 31). Surprisingly, the extent of staining and layer widths observed by transmission electron microscopy (TEM) are completely inconsistent with both the side-chain volume fractions measured by ^{1}H NMR ($f_L = 0.57$, $f_S = 0.37$, $f_O = 0.06$) (Fig. 2*B*) and the ABCB connectivity required by the expected three-domain microstructure, LAM_3 (Fig. 2*C*) (8, 9). The conflict between LAM_3 and the pattern observed by TEM can only be resolved by invoking partial mixing between the A and C end blocks, apparently driven by low-χ interactions ($\chi_{AC} \lesssim 0$). The resulting morphology exhibits mesoscopic ACBC connectivity (Fig. 2*D*), consistent with the observed staining pattern. Because the three blocks are not well-segregated, the side-chain volume fractions are not required to equal the relative domain widths. Reflecting the crucial role of partial mixing, this unique morphology is herein designated LAM_P.

SCFT fully supports the distinction between LAM_3 (Fig. 3*A*) and LAM_P (Fig. 3*B*), controlled primarily by the relative and absolute interaction parameters. Composition profiles for LSO* were calculated over one lamellar period using realistic PLA–PS ($\chi_{AB} \equiv \chi_{LS}$) and PS–PEO ($\chi_{BC} \equiv \chi_{SO}$) values estimated in the literature: $\chi_{LS} = 0.080$ (32) and $\chi_{SO} = 0.049$ (33) at 140 °C, renormalized to a common monomer reference volume (118 Å^3). (We note that literature χ-values obtained by fitting experimental data to mean-field approximations are often inaccurate, potentially affecting the agreement between experiment and theory (34).) PLA–PEO interactions ($\chi_{AC} \equiv \chi_{LO}$) were arbitrarily varied in the simulations, and LAM_3 is correctly predicted to occur at moderate to large χ_{AC} (Fig. 3*C*), in broad agreement with previous experimental and theoretical studies of frustrated ABC triblock terpolymers (35–37). In contrast, LAM_P exclusively emerges when χ_{AC} is sufficiently small to favor partial A/C block–block mixing (Fig. 3*D*). Using this collection of physical parameters, a first-order phase transition between LAM_3 and

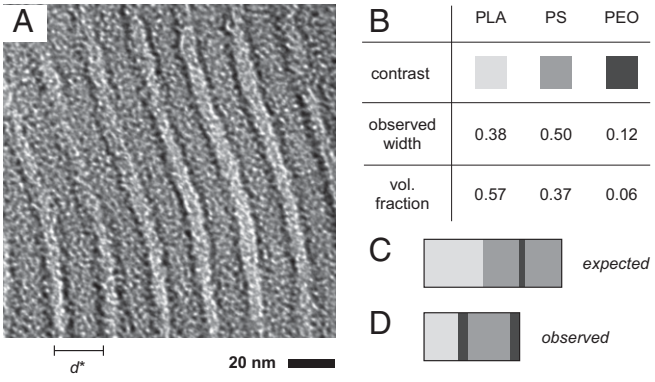

Fig. 2. (*A*) TEM of LSO* stained with RuO_4. (*B*) Relative contrast from the stain, relative widths of corresponding layers observed by TEM, and side-chain volume fractions measured by ^{1}H NMR. (*C*) One LAM_3 period with the expected ABCB domain connectivity and layer widths based on data in *B*. (*D*) One LAM_P period observed in *A*, exhibiting mesoscopic ACBC domain connectivity.

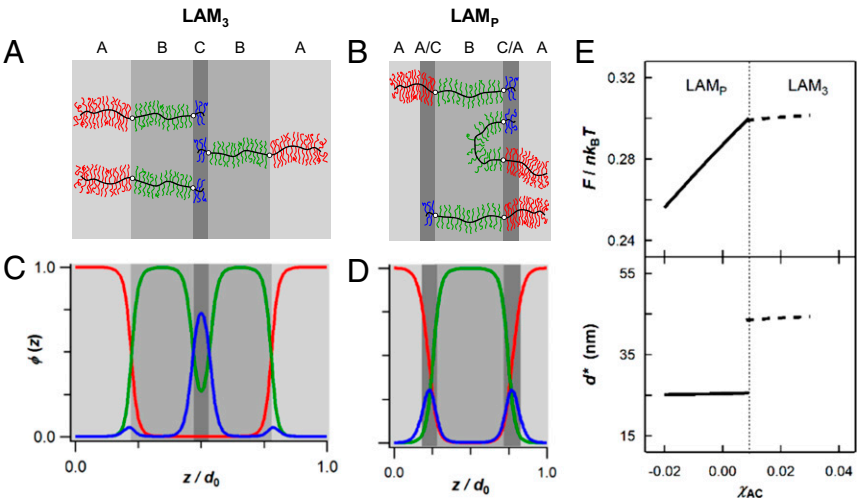

Fig. 3. Illustrations and SCFT data distinguishing LAM_3 and LAM_P morphologies. In *A–D*, the light-, medium-, and dark-gray layers represent PLA, PS, and PEO (or mixed PLA/PEO) domains, respectively. (*A* and *B*) LSO chain packing in (*A*) LAM_3 and (*B*) LAM_P. (*C* and *D*) SCFT composition profiles for LSO* within one normalized lamellar period (z/d_0), where $\phi(z)$ is the relative segment concentration of each component. (*C*) $\chi_{AC} > \chi^C$: LAM_3 with $d^* = 43.5$ nm. (*D*) $\chi_{AC} < \chi^C$: LAM_P with $d^* = 25.6$ nm. (*E*) SCFT calculations of the normalized free energy (*Top*) and domain spacing (*Bottom*) versus $\chi_{AC} \equiv \chi_{LO}$ for LSO*. The transition from mixed (LAM_P) to unmixed (LAM_3) morphologies is first order, occurring at a critical value χ^C (dotted line); for $\chi_{AB} = 0.080$ and $\chi_{BC} = 0.049$, $\chi^C = 0.009$.

LAM_P was predicted to occur at a critical value $\chi^C = 0.009$ (Fig. 3*E*). The mesoscopic ACBC domain connectivity and relative domain widths predicted for LAM_P perfectly match the pattern observed in Fig. 2*A* and reinforce the microscopic origins of mixing deduced from TEM.

Decreasing Domain Spacing with Increasing Total Molar Mass. A series of LSO brush triblock terpolymers with fixed $N_A = 26$ and $N_B = 24$ (guaranteed by a common parent diblock) and variable N_C (*SI Appendix*, Scheme S3) highlights additional consequences of block–block mixing. N_C was varied in increments of two or four backbone repeat units, from $N_C = 0$ (LSO-0) to $N_C = 20$ (LSO-20) (*SI Appendix*, Table S1). (Note that, due to the high molar mass of each PEO macromonomer, the total molar mass varies by >45,000 g/mol across this series.) SAXS measurements reveal an unusual trend: as the total molar mass (M) increases over the range of compositions where LAM_P forms ($0 < f_O \lesssim 0.20$), the lamellar period (d^*) strongly decreases: $d^* \sim M^{-0.87}$ (Fig. 4*A*). For comparison, Fig. 4*A* also includes literature data for linear poly(isoprene-*b*-styrene-*b*-ethylene oxide) (ISO) and poly(styrene-*b*-isoprene-*b*-ethylene oxide) (SIO) triblock terpolymers similarly synthesized by varying the O block length from a common parent diblock. The domain spacing trends observed for both ISO and SIO series typify the expected increase in lamellar period with increasing M: $\alpha_{ISO} \approx 0.90$ (38, 39) and $\alpha_{SIO} \approx 0.56$ (40). Clearly, α_{LSO} is strikingly different. Additional data illustrating the unusual negative trend for LSO are summarized in the *SI Appendix*, Table S4. Schematic illustrations of assigned structures (*SI Appendix*, Fig. S6), indexed 2D SAXS data (*SI Appendix*, Fig. S7), 1D azimuthally averaged intensity reductions (*SI Appendix*, Fig. S8), and TEM images (*SI Appendix*, Fig. S9) are also provided.

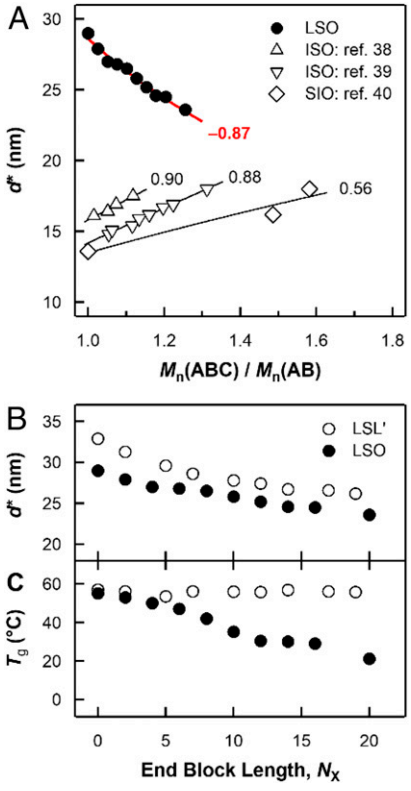

Fig. 4. (*A*) Lamellar periods (d^*) versus normalized molar mass for brush LSO (this work) and linear ISO and SIO triblock terpolymers (literature data). Calculated exponents (best fit) to the power law $d^* \sim M^{\alpha}$ are included for comparison. (*B* and *C*) Consequences of varying end-block length N_X in LSL′ and LSO. (*B*) Domain spacing d^*. (*C*) Apparent PLA glass transition temperatures (T_g); for all samples, a single T_g ($T_{g,PEO} < T_g \leq T_{g,PLA}$) was observed.

A series of LSL′ brush triblock copolymers was similarly synthesized from identical macromonomers, generating an analogous series with variable end-block length from a parent LS diblock ($N_A = 30$, $N_B = 28$). Like LSO, this LSL′ series exhibits decreasing lamellar periods with increasing end-block length (i.e., increasing total molar mass) (Fig. 4*B*). Additional morphological data for LSL′ are provided in the *SI Appendix*, Table S5 and Figs. S10 and S11. Differential scanning calorimetry data for LSL′ and LSO are compared in Fig. 4*C* and provide quantitative evidence of block–block mixing in LSO. For all LSO samples, a single glass transition temperature (T_g) was observed between $T_{g,PLA}$ (55 °C) and $T_{g,PEO}$ (−70 °C) (*SI Appendix*, Fig. S12). As N_C (and therefore the weight fraction of PEO) increases, T_g decreases, consistent with continued dilution of mixed A/C domains by the low-T_g component. The presence of only one T_g in polymer blends is generally regarded as evidence for miscibility (41, 42) and is consistent with the behavior of PLA and PEO homopolymers, which mix over wide ranges of molar masses and blend compositions (43, 44). In the analogous LSL′ series, a single T_g corresponding to the PLA block is observed that does not change as $N_{A'}$ increases, because mixed domains inherently remain pure PLA (*SI Appendix*, Fig. S13).

Role of Low-χ Interactions. We have investigated herein the impact of low-χ block–block interactions on structure and physical properties by studying densely grafted ABC and ABA′ brush triblock polymers. The LSO polymers described above self-assemble into lamellae with unique domain connectivity (ACBC), which we denote LAM_P. In

contrast, linear ABC triblock terpolymers (e.g., ISO and SIO) have been extensively studied and typically form two- or three-domain lamellar morphologies (LAM_2 or LAM_3) depending on block lengths and relative interaction parameters. In the conventional LAM_3 morphology generated by both ISO and SIO, the mesoscopic domain connectivity (ABCB) necessarily reflects the underlying molecular sequence. In other words, the self-assembly of ABC… multiblock polymers into lamellae (i.e., structures periodic in one dimension) typically requires A, B, C, … domains to be connected in that order due to the covalent linkages between blocks. The crucial differences distinguishing LSO and ostensibly similar ISO/SIO triblocks could potentially be attributed to either the polymer architecture (brush vs. linear) or block–block interactions. We note that architecture-induced segmental mixing has been demonstrated in ABC heteroarm star terpolymers, wherein forming low-energy morphologies may force one arm to transit across an incompatible domain ($\chi > 0$) (45, 46). However, these architecture effects do not pertain to brush LSO because the blocks are connected end-to-end in the same way as linear ABC triblock terpolymers. The data presented in Figs. 2–4 instead indicate that block–block interactions, captured through the mean-field concept of Flory–Huggins binary interaction parameters (χ_{ij}), are the dominant factors governing the unique behavior of LSO.

Both the relative and absolute magnitudes of each χ_{ij}, convolved with the molecular sequence, underpin the self-assembly of multiblock polymers. For example, given I, S, and O blocks with $\chi_{IO} > \chi_{IS} \approx \chi_{SO}$ (47, 48), SIO connectivity imposes costly high-χ interactions between adjacent blocks ($\chi_{BC} > \chi_{AB} \approx \chi_{AC}$), whereas ISO connectivity alleviates this penalty by not inherently requiring I/O (A/C) interfaces. ISO and SIO phase diagrams are consequently distinct due to so-called frustration. The influence of each χ_{ij} is less understood. In contrast to (SI/IS)O materials where every $\chi_{ij} >> 0$, the LSO polymers studied herein feature low χ_{AC} between the end blocks ($\chi_{LO} \lesssim 0$). Actual literature estimates for χ_{LO} range from 0.0038 to –0.161 depending on end groups and measurement techniques (49, 50). Combining any $-0.161 < \chi_{LO} < 0.0038$ with the aforementioned literature values $\chi_{LS} = 0.080$ and $\chi_{SO} = 0.049$ yields a frustrated system. SCFT simulations (Fig. 3) suggest that the magnitude of χ_{LO}, beyond simple frustration effects, dictates the unique LAM_P self-assembly observed in Fig. 2. Calculations for LSO indicate that LAM_P is stable when $\chi_{LO} < \chi^C$, which marks a first-order phase transition between LAM_P and LAM_3 (Fig. 3*E*). The predicted value of χ^C is sensitive to physical parameters including the statistical segment lengths and χ_{ij} and is consequently difficult to quantitatively associate with experiments. Using the aforementioned literature values corresponding to L, S, and O pairwise interactions, we estimate $\chi^C \sim 0.009$, which sets an approximate upper bound on the value of χ_{LO} because no evidence of LAM_3 is experimentally observed. Experiment and theory collectively suggest that low-χ interactions ($\chi_{AC} \lesssim 0$) underpin the self-assembly of LSO to LAM_P.

Molecular Asymmetry Effects. The pronounced decrease in domain spacing observed for LSO and LSL′ upon increasing N_C or $N_{A'}$ (at constant N_A, N_B) also emerges as a consequence of the low-χ design, involving molecular asymmetry, block–block mixing, and screening effects. SCFT simulations of linear ABA′ triblock copolymers have previously revealed that asymmetry in A/A′ block lengths can induce a decrease in domain spacing (51). The explanation is twofold. First, A/A′ asymmetry lowers the stretching energy in A domains (52), which can be understood by imagining equivalent A block lengths and then transferring material from one end to the other; as asymmetry increases, the overall A segment distribution shifts away from the interface, increasing d^*. Second, when the end blocks are sufficiently asymmetric, a significant proportion of the shorter A blocks can pull out into B domains (Fig. 5*A*). Although chain pullout incurs an enthalpic penalty ($\chi_{AB} > 0$), this effect is more than compensated by relaxation of the B block, which is entropically favored and further increases d^*. The synthesis of ABA′ triblocks from a common diblock precursor exhibits the same trend: growing longer A′ blocks decreases molecular asymmetry and correspondingly lowers d^*. Experimental studies of linear ABA′ triblock copolymers have corroborated this theory of end-block asymmetry (53, 54), and the LSL′ and LSO brush triblock polymers studied herein exhibit strikingly similar behavior. We conclude that architecture is not a critical molecular design parameter dictating the trends in d^* (Fig. 4); instead, the close parallels between the self-assembly of ABA′ triblock copolymers and appropriately designed ABC triblock terpolymers implicate block–block mixing. ABA′ samples (linear or brush) clearly have mixed A/A′ domains before chain pullout, and a negligible χ_{LO} in LSO should also promote end-block mixing. Application of the stretching energy and chain pullout concepts developed to rationalize ABA′ self-assembly therefore also captures the essence of ABC systems (Fig. 5*B*). Molar mass dispersity additionally favors pullout of shorter end blocks (A′ or C), whereas longer ones remain anchored in mixed domains.

Informed SCFT simulations of LSO indicate the stability of LAM_P over a wide range of N_C (*SI Appendix*, Fig. S14). In addition, simulations incorporating an exponential distribution of end-block dispersity for both LSO and LSL′ (*SI Appendix*, Tables S6 and S7) show good agreement between the predicted and measured magnitudes of d^*. The simulations capture a sharp initial decrease in d^* when the backbone lengths of the third block are short (N_C, $N_{A'} \leq 7$), reinforcing the significance of molecular asymmetry and chain pullout. As the end-block lengths continue to increase, however, the predicted values of d^* monotonically increase, in contrast to the experimental trends. These disparities may reflect (*i*) inaccuracies in the χ_{ij} values used (34), (*ii*) larger dispersities in N_C and $N_{A'}$ than anticipated by theory, or (*iii*) potential nonequilibrium effects, as discussed below.

Screening Unfavorable Block–Block Interactions. In LSO, the effects of molecular asymmetry and chain pullout are amplified by the screening of high-χ block–block interactions. The most unfavorable contacts in LSO (L/S) can be partially mitigated by inserting PEO between PLA and PS domains near the interface, because $\chi_{LS} > \chi_{SO}$ and $\chi_{LO} \lesssim 0$. This possibility is naturally permitted in the disordered state, but upon self-assembly to the conventional LAM_3 morphology, chain connectivity necessarily creates energetically costly PLA/PS interfaces. Screening L/S contacts in LAM_3 would typically require altering the block sequence to LOS, an impossible task postsynthesis, but LAM_P restores this opportunity by incorporating partial mixing between the end blocks. This phenomenon decouples the molecular block sequence from the self-assembled domain pattern. Screening unfavorable block–block interactions in LSO likely also contributes to the molecular origins of the domain spacing trend. As PEO inserts between PLA and PS blocks at the interface, it should expand the intermolecular distance in the plane of the lamellae and therefore contract the lamellar period (i.e., d^*). Similar mixing consequences have been observed in block polymer/homopolymer blends in which the homopolymer localizes at the block–block interfaces (55–57).

Dispersity, Crystallization, and Architecture. Comparing LSO, LSL′, and linear (IS/SI)O reinforces the importance of low-χ interactions and refutes other potential explanations for the unique mesoscopic ACBC domain connectivity and domain spacing trend. Dispersity differences among the blocks can be discounted because all samples across the LSO, LSL′, ISO, and SIO series depicted in Fig. 4 were synthesized by living polymerizations (either ROMP or anionic polymerization) from parent diblock precursors. Because O comprises the C block in each ABC series, PEO clearly does not inherently cause domain contraction with increasing O block lengths or weight fractions. Furthermore, we see little evidence of extensive PEO crystallization from variable-temperature wide-angle X-ray scattering data, which indicate that all LSO LAM_P samples contain low crystalline weight fractions (<10 wt %) (*SI Appendix*, Figs. S15 and S16). Densification upon PEO crystallization and concomitant domain contraction is therefore unlikely. The higher molar mass O blocks in linear ISO and SIO would presumably accentuate this effect, yet both ISO and SIO show strong increases in d^* with N_C. Comparing LSO and LSL′ provides further evidence that crystallization is not

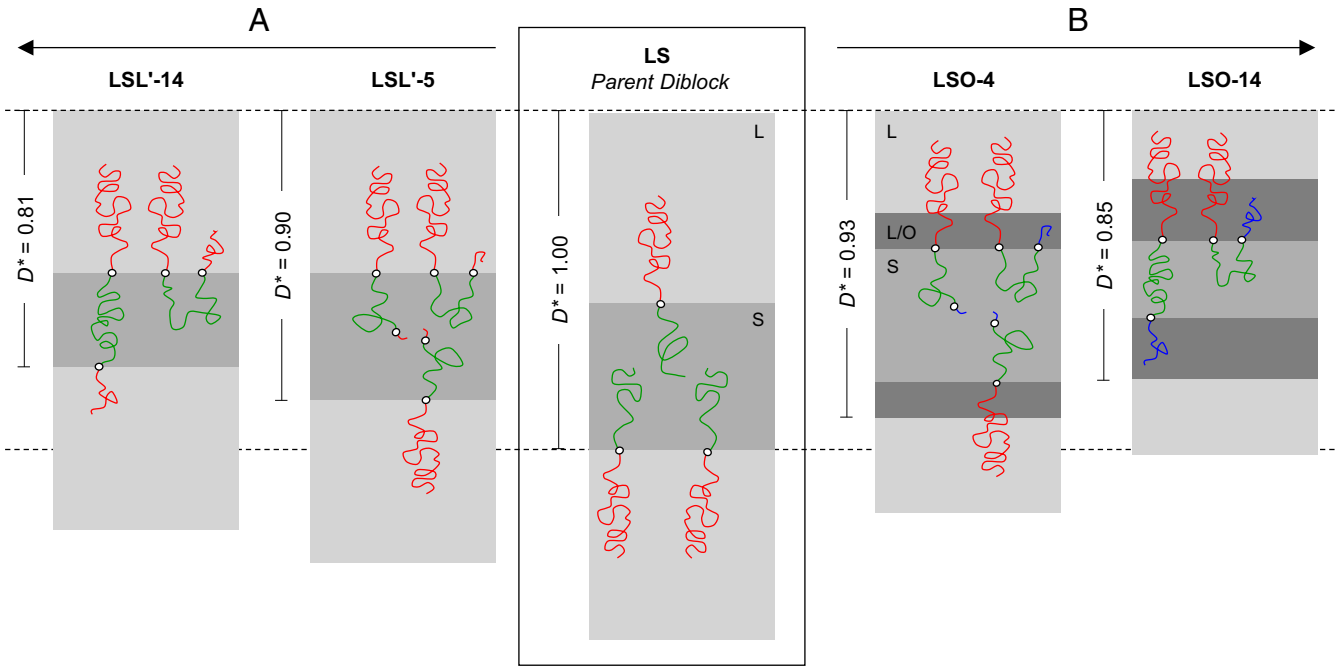

Fig. 5. Illustration of chain pullout to explain the trends in d^* for LSL′ and LSO brush triblock polymers with varying end-block length (equivalently, varying molecular asymmetry). Linear chains are depicted to aid visualization. As the end-block length N_X increases from a fixed parent LS diblock, d^* decreases (here, $D^* \equiv d^*/d^*_{LS}$, where d^*_{LS} is the period of the parent LS diblock). (*A*) X = A′ (LSL′): short PLA end blocks pull out of PLA domains into PS domains. (*B*) X = C (LSO): short PEO end blocks pull out of mixed PLA/PEO domains into PS domains.

responsible for the unusual trend in d^*: Whereas both LSO and LSL′ exhibit decreasing d^* with increasing end-block lengths, LSL′ has no crystallizable components.

We expect that the phenomena described above, illustrating the physical consequences of designing polymers with certain miscible blocks, are general to the class of soft materials with χ_{AB}, $\chi_{BC} >> |\chi_{AC}| \approx 0$. Although bottlebrush polymers were used in the present study, SCFT calculations predict identical behavior for analogous linear triblock terpolymers with the same absolute and relative χ-parameters (*SI Appendix*, Fig. S17). Although bottlebrush polymers experience some steric-induced stiffening compared to linear polymers (58, 59), our results suggest that brush LSO and LSL′ are actually relatively flexible. The backbone flexibility should enable brush LS(O/L′) to adopt looping midblock configurations (Figs. 3 and 5), just like linear AB(C/A′) triblocks with compatible end blocks (60, 61). Informed SCFT calculations indicate that the effective backbone persistence length of brush LSO and LSL′ corresponds to ~5 norbornene repeat units (25). Because the B midblocks of LSO and LSL′ are much longer than 5 units ($N_B \geq 24$), they should readily form loops, although undoubtedly less than the 40% predicted for flexible (linear) triblocks (62). Our results, placed in the context of recent work on bottlebrush block polymer self-assembly, suggest that polymer architecture is not a major factor controlling the formation of partially mixed morphologies. Instead, the primary driving force appears to be the magnitude of χ_{AC}. Designed low-χ interactions emerge as tools to manipulate block polymer self-assembly.

Potential Nonequilibrium Behavior. Although SCFT calculations suggest that LAM_P is at equilibrium with experimentally relevant values of χ and f, experimental proof is currently limited by our inability to access the order–disorder transition temperature (T_{ODT}). SAXS data obtained upon heating a LAM_P sample (LSO with $N_A = 25$, $N_B = 22$, $N_C = 5$) from 25 to 200 °C indicate that LAM_P is thermally stable throughout the entire experimentally accessible temperature range (*SI Appendix*, Fig. S18). Consistent with other reports of high-molar-mass bottlebrush polymers (25, 63), no T_{ODT} is observed below the onset of decomposition, preventing careful annealing and quench studies originating from the disordered state. Because SCFT is an equilibrium theory, any deviations from equilibrium would affect the agreement between experimentally measured results and predicted behavior.

To further probe potential nonequilibrium effects and because morphologies for multiblock polymers can be sensitive to processing conditions (64, 65), an LSO brush triblock terpolymer ($N_A = 25$, $N_B = 22$, $N_C = 5$) was annealed in four different ways: thermal annealing under pressure, thermal annealing without pressure, drop casting, and channel die alignment. All approaches afforded self-assembled morphologies with virtually identical LAM_P geometry and periodicity (±0.5 nm) (*SI Appendix*, Fig. S19). These results are reported while acknowledging studies of linear multiblock polymers that highlight the potential influence of processing path on the formation of kinetically trapped structures (66, 67), which may be mistaken for equilibrium. Previously, ABC block polymer morphologies containing partially mixed regions have indeed been predicted (68) and observed (69) as metastable defect states kinetically trapped upon casting from preferential solvents, but these examples were easily annihilated during the type of extended thermal treatments performed herein to anneal LSO. Equilibrium or not, the morphological attributes of LAM_P are long-lived, in contrast to and notably distinct from prior materials.

Conclusion

The insights gained herein from both experiment and theory illustrate the profound influence low-χ interactions exert on self-assembly. Proper selection of χ_{ij} and f can generate unusual morphologies characterized by partial block mixing (LAM_P), decouple molecular sequence from mesoscopic connectivity, and provide counterintuitive control over domain spacing. Whereas high-χ block polymers have been the subject of widespread interest, low-χ systems remain relatively unexplored, yet the latter generate fascinating physics that are anticipated to gain importance as sequence complexity further evolves. Expanding the block polymer design toolkit to include low-χ interactions creates new opportunities to tailor mesoscale structure and should find utility in the future design of functional materials.

ACKNOWLEDGMENTS. The authors thank M. S. Ladinsky for assistance with ultramicrotomy, as well as M. T. Irwin, S. Chanpuriya, and T. Li for helpful discussions about sample preparation and TEM. The authors gratefully acknowledge helpful discussions with F. S. Bates and Z.-G. Wang. This work was supported by the National Science Foundation through Grant CHE-1502616. A.B.C. thanks the US Department of Defense for support through the National Defense Science and Engineering Graduate (NDSEG) Fellowship. C.M.B. thanks the Dreyfus Foundation for Environmental Postdoctoral Fellowship EP-13-142 and the University of California, Santa Barbara for funding. This research used resources of the Advanced Photon Source, a US Department of Energy Office of Science User Facility operated by Argonne National Laboratory under Contract DE-AC02-06CH11357.

1. Thomas EL (1999) The ABCs of self-assembly. *Science* 286:1307.
2. Park C, Yoon J, Thomas EL (2003) Enabling nanotechnology with self assembled block copolymer patterns. *Polymer (Guildf)* 44:6725–6760.
3. Lutz J-F, Ouchi M, Liu DR, Sawamoto M (2013) Sequence-controlled polymers. *Science* 341:1238149.
4. Bates CM, Bates FS (2016) 50th anniversary perspective: Block polymers—pure potential. *Macromolecules* 50:3–22.
5. Leibler L (1980) Theory of microphase separation in block copolymers. *Macromolecules* 13: 1602–1617.
6. Bates FS, Fredrickson GH (1999) Block copolymers—designer soft materials. *Phys Today* 52:32–38.
7. Bates FS, et al. (2012) Multiblock polymers: Panacea or Pandora's box? *Science* 336:434–440.
8. Zheng W, Wang Z-G (1995) Morphology of ABC triblock copolymers. *Macromolecules* 28:7215–7223.
9. Bailey TS (2001) Morphological behavior spanning the symmetric AB and ABC block copolymer states. PhD thesis (University of Minnesota, Minneapolis).
10. Xie N, et al. (2014) Macromolecular metallurgy of binary mesocrystals via designed multiblock terpolymers. *J Am Chem Soc* 136:2974–2977.
11. Gao Y, Deng H, Li W, Qiu F, Shi A-C (2016) Formation of nonclassical ordered phases of AB-type multiarm block copolymers. *Phys Rev Lett* 116:068304.
12. Legge NR (1987) Thermoplastic elastomers. *Rubber Chem Technol* 60:83–117.
13. Bluemle MJ, Zhang J, Lodge TP, Bates FS (2010) Inverted phases induced by chain architecture in ABAC tetrablock terpolymers. *Macromolecules* 43:4449–4452.
14. Lee S, Bluemle MJ, Bates FS (2010) Discovery of a Frank-Kasper σ phase in sphere-forming block copolymer melts. *Science* 330:349–353.
15. Lynd NA, Oyerokun FT, O'Donoghue DL, Handlin DL, Fredrickson GH (2010) Design of soft and strong thermoplastic elastomers based on nonlinear block copolymer architectures using self-consistent-field theory. *Macromolecules* 43:3479–3486.
16. Hashimoto T, Tanaka H, Hasegawa H (1990) Ordered structure in mixtures of a block copolymer and homopolymers. 2. Effects of molecular weights of homopolymers. *Macromolecules* 23:4378–4386.
17. Matsen MW (1995) Phase behavior of block copolymer/homopolymer blends. *Macromolecules* 28:5765–5773.
18. Kimishima K, Jinnai H, Hashimoto T (1999) Control of self-assembled structures in binary mixtures of A–B diblock copolymer and A–C diblock copolymer by changing the interaction between B and C block chains. *Macromolecules* 32:2585–2596.
19. Tang C, et al. (2010) Multiple nanoscale templates by orthogonal degradation of a supramolecular block copolymer lithographic system. *ACS Nano* 4:285–291.
20. Sveinbjörnsson BR, et al. (2012) Rapid self-assembly of brush block copolymers to photonic crystals. *Proc Natl Acad Sci USA* 109:14332–14336.
21. Bates CM, Chang AB, Momčilović N, Jones SC, Grubbs RH (2015) ABA triblock brush polymers: Synthesis, self-assembly, conductivity, and rheological properties. *Macromolecules* 48:4967–4973.
22. Bates CM, et al. (2016) Brush polymer ion gels. *J Polym Sci, B, Polym Phys* 54:292–300.
23. Radlauer MR, et al. (2016) Morphological consequences of frustration in ABC triblock polymers. *Macromolecules* 50:446–458.
24. Fredrickson GH (2006) *The Equilibrium Theory of Inhomogeneous Polymers* (Oxford Univ Press, New York).
25. Dalsin SJ, et al. (2015) Bottlebrush block polymers: Quantitative theory and experiments. *ACS Nano* 9:12233–12245.
26. Fetters LJ, Lohse DJ, Richter D, Witten TA, Zirkel A (1994) Connection between polymer molecular weight, density, chain dimensions, and melt viscoelastic properties. *Macromolecules* 27:4639–4647.
27. Dorgan JR, et al. (2005) Fundamental solution and single-chain properties of polylactides. *J Polym Sci, B, Polym Phys* 43:3100–3111.
28. Olayo-Valles R, Lund MS, Leighton C, Hillmyer MA (2004) Large area nanolithographic templates by selective etching of chemically stained block copolymer thin films. *J Mater Chem* 14:2729–2731.
29. Vayer M, Nguyen TH, Sinturel C (2014) Ruthenium staining for morphological assessment and patterns formation in block copolymer films. *Polymer (Guildf)* 55:1048–1054.
30. Trent JS, Scheinbeim JI, Couchman PR (1983) Ruthenium tetraoxide staining of polymers for electron microscopy. *Macromolecules* 16:589–598.
31. Gai Y, Song D-P, Yavitt BM, Watkins JJ (2017) Polystyrene-block-poly(ethylene oxide) bottlebrush block copolymer morphology transitions: Influence of side chain length and volume fraction. *Macromolecules* 50:1503–1511.
32. Zalusky AS, Olayo-Valles R, Wolf JH, Hillmyer MA (2002) Ordered nanoporous polymers from polystyrene-polylactide block copolymers. *J Am Chem Soc* 124:12761–12773.
33. Cochran EW, Morse DC, Bates FS (2003) Design of ABC triblock copolymers near the ODT with the random phase approximation. *Macromolecules* 36:782–792.
34. Beardsley TM, Matsen MW (2016) Universality between experiment and simulation of a diblock copolymer melt. *Phys Rev Lett* 117:217801.
35. Stadler R, et al. (1995) Morphology and thermodynamics of symmetric poly(A-*block*-B-*block*-C) triblock copolymers. *Macromolecules* 28:3080–3097.
36. Balsamo V, et al. (2003) Morphological behavior of thermally treated polystyrene-*b*-polybutadiene-*b*-poly(ε-caprolactone) ABC triblock copolymers. *Macromolecules* 36:4515–4525.
37. Liu M, Li W, Qiu F, Shi A-C (2012) Theoretical study of phase behavior of frustrated ABC linear triblock copolymers. *Macromolecules* 45:9522–9530.
38. Bailey TS, Hardy CM, Epps TH, Bates FS (2002) A noncubic triply periodic network morphology in poly(isoprene-b-styrene-b-ethylene oxide) triblock copolymers. *Macromolecules* 35:7007–7017.
39. Meuler AJ, et al. (2009) Polydispersity effects in poly(isoprene-b-styrene-b-ethylene oxide) triblock terpolymers. *J Chem Phys* 130:234903.
40. Bailey TS, Pham HD, Bates FS (2001) Morphological behavior bridging the symmetric AB and ABC states in the poly(styrene-b-isoprene-b-ethylene oxide) triblock copolymer system. *Macromolecules* 34:6994–7008.
41. Couchman PR (1978) Compositional variation of glass-transition temperatures. 2. Application of the thermodynamic theory to compatible polymer blends. *Macromolecules* 11: 1156–1161.
42. Gaikwad AN, Wood ER, Ngai T, Lodge TP (2008) Two calorimetric glass transitions in miscible blends containing poly(ethylene oxide). *Macromolecules* 41:2502–2508.
43. Younes H, Cohn D (1988) Phase separation in poly(ethylene glycol)/poly(lactic acid) blends. *Eur Polym J* 24:765–773.
44. Sheth M, Kumar RA, Davé V, Gross RA, McCarthy SP (1997) Biodegradable polymer blends of poly(lactic acid) and poly(ethylene glycol). *J Appl Polym Sci* 66:1495–1505.
45. Sioula S, Hadjichristidis N, Thomas EL (1998) Novel 2-dimensionally periodic nonconstant mean curvature morphologies of 3-miktoarm star terpolymers of styrene, isoprene, and methyl methacrylate. *Macromolecules* 31:5272–5277.
46. Tang P, Qiu F, Zhang H, Yang Y (2004) Morphology and phase diagram of complex block copolymers:ABC star triblock copolymers. *J Phys Chem B* 108:8434–8438.
47. Frielinghaus H, et al. (2001) Micro- vs. macro-phase separation in binary blends of poly(styrene)-poly(isoprene) and poly(isoprene)-poly(ethylene oxide) diblock copolymers. *Europhys Lett* 53:680–686.
48. Chatterjee J, Jain S, Bates FS (2007) Comprehensive phase behavior of poly(isoprene-b-styrene-b-ethylene oxide) triblock copolymers. *Macromolecules* 40:2882–2896.
49. Mao H, Hillmyer MA (2008) Morphological behavior of polystyrene-block-polylactide/polystyrene-block-poly(ethylene oxide) blends. *Macromol Chem Phys* 209:1647–1656.
50. Lai W-C, Liau W-B, Lin T-T (2004) The effect of end groups of PEG on the crystallization behaviors of binary crystalline polymer blends PEG/PLLA. *Polymer (Guildf)* 45:3073–3080.
51. Matsen MW (2000) Equilibrium behavior of asymmetric ABA triblock copolymer melts. *J Chem Phys* 113:5539–5544.
52. Milner ST, Witten TA (1988) Bending moduli of polymeric surfactant interfaces. *J Phys France* 49:1951–1962.
53. Hamersky MW, Smith SD, Gozen AO, Spontak RJ (2005) Phase behavior of triblock copolymers varying in molecular asymmetry. *Phys Rev Lett* 95:168306.
54. Smith SD, Hamersky MW, Bowman MK, Rasmussen KØ, Spontak RJ (2006) Molecularly asymmetric triblock copolymers as a single-molecule route to ordered bidisperse polymer brushes. *Langmuir* 22:6465–6468.
55. Winey KI, Thomas EL, Fetters LJ (1991) Swelling of lamellar diblock copolymer by homopolymer: Influences of homopolymer concentration and molecular weight. *Macromolecules* 24:6182–6188.
56. Koizumi S, Hasegawa H, Hashimoto T (1994) Spatial distribution of homopolymers in block copolymer microdomains as observed by a combined SANS and SAXS method. *Macromolecules* 27:7893–7906.
57. Chen S-C, Kuo S-W, Jeng US, Su C-J, Chang F-C (2010) On modulating the phase behavior of block copolymer/homopolymer blends via hydrogen bonding. *Macromolecules* 43:1083–1092.
58. Fredrickson GH (1993) Surfactant-induced lyotropic behavior of flexible polymer solutions. *Macromolecules* 26:2825–2831.
59. Mikhaylov IV, Darinskii AA (2015) Effect of the side-arm architecture on the conformational properties of bottle brushes. *Polym Sci Ser A* 57:239–250.
60. Zhulina EB, Halperin A (1992) Lamellar mesogels and mesophases: A self-consistent-field theory. *Macromolecules* 25:5730–5741.
61. Kane L, Spontak RJ (1994) Microstructural characteristics of strongly-segregated AXB triblock terpolymers possessing the lamellar morphology. *Macromolecules* 27:1267–1273.
62. Matsen MW, Thompson RB (1999) Equilibrium behavior of symmetric ABA triblock copolymer melts. *J Chem Phys* 111:7139–7146.
63. Xia Y, Olsen BD, Kornfield JA, Grubbs RH (2009) Efficient synthesis of narrowly dispersed brush copolymers and study of their assemblies: The importance of side chain arrangement. *J Am Chem Soc* 131:18525–18532.
64. Mori K, Hasegawa H, Hashimoto T (1990) Ordered structure in block polymer solutions: 6. Possible non-equilibrium effects on growth of self-assembling structures. *Polymer (Guildf)* 31:2368–2376.
65. Lodge TP, Pudil B, Hanley KJ (2002) The full phase behavior for block copolymers in solvents of varying selectivity. *Macromolecules* 35:4707–4717.
66. Lipic PM, Bates FS, Matsen MW (1999) Non-equilibrium phase behavior of diblock copolymer melts and binary blends in the intermediate segregation regime. *J Polym Sci, B, Polym Phys* 37:2229–2238.
67. Chanpuriya S, et al. (2016) Cornucopia of nanoscale ordered phases in sphere-forming tetrablock terpolymers. *ACS Nano* 10:4961–4972.
68. Xia J, Sun M, Qiu F, Zhang H, Yang Y (2005) Microphase ordering mechanisms in linear ABC triblock copolymers. A dynamic density functional study. *Macromolecules* 38:9324–9332.
69. Corté L, et al. (2003) Annealing and defect trapping in lamellar phases of triblock terpolymers. *Macromolecules* 36:7695–7706.